ISSN 0023-1584, Kinetics and Catalysis, 2015, Vol. 56, No. 6, pp. 758–763. © Pleiades Publishing, Ltd., 2015.
Original Russian Text © T.A. Bugrova, N.N. Litvyakova, G.V. Mamontov, 2015, published in Kinetika i Kataliz, 2015, Vol. 56, No. 6, pp. 746–752.

Effect of Zirconia Additives on the Activity of the Cr/SiO_2 Catalyst in Isobutane Dehydrogenation

T. A. Bugrova, N. N. Litvyakova, and G. V. Mamontov*

Tomsk State University, Tomsk, 634050 Russia

**e-mail: GrigoriyMamontov@mail.ru*

Received November 26, 2014

Abstract—A new approach to the preparation of modified silica-based supports is suggested to obtain Cr-containing catalysts for paraffin hydrocarbon dehydrogenation. CrO_x/ZrO_2, CrO_x/SiO_2, and $CrO_x/nZrO_2$–SiO_2 (n = 0.5, 1.0, and 2.0 ZrO_2 monolayers) catalysts have been synthesized by incipient-wetness impregnation. The catalysts have been characterized by X-ray diffraction, diffuse reflectance spectroscopy, and temperature-programmed reduction with hydrogen. Their catalytic properties were investigated in the reaction of isobutane dehydrogenation. The state of the supported chromium depends considerably on the nature of the support. The formation of Cr_2O_3 particles, which show low activity in the dehydrogenation reaction, takes place in the CrO_x/SiO_2 catalyst, while chromium in the CrO_x/ZrO_2 catalyst is in a highly dispersed, X-ray-amorphous state. The addition of ZrO_2 to CrO_x/SiO_2 increases the amount of chromium in the highly dispersed Cr(V) and Cr(VI) states, thus enhancing the isobutane dehydrogenation activity of the catalyst.

Keywords: chromium-containing catalysts, mixed supports, ZrO_2, SiO_2, isobutane dehydrogenation

DOI: 10.1134/S0023158415060014

At present, reactions of catalytic paraffin hydrogenation are of great importance for the chemical and petrochemical industries. There are different engineering and technological implementations of dehydrogenation processes: fluidized catalyst bed (Yarsintez process), fixed catalyst bed (Catofin and Catadiene processes), nonoxidative and oxidative dehydrogenation, etc. [1–5]. Dehydrogenation can be carried out over a variety of catalysts, namely, metal oxide [6–8] and phosphorus- and platinum-containing ones [9, 10]. The most common catalysts employed in the dehydrogenation of C_4 and C_5 hydrocarbons are chromium-containing systems. The state of supported chromium and, hence, its catalytic properties are determined by the properties of the support and catalyst preparation conditions. By varying the nature of the support or introducing an additivet, it is possible to control the state of the supported active component. The most common support for chromium-containing systems is γ-Al_2O_3, because of its availability and inexpensiveness, the possibility of shaping it into granules of various shapes and sizes, capability to stabilize chromium in the active highly dispersed state, high porosity and large specific surface area. In the Russian industry, γ-Al_2O_3 is used as the support for the following catalysts: AOK-73-21 (RF Specifications TU 6-68-170-00), AOK-73-24, IM-2201 (USSR Specifications TU 38.103706-90), and KDM [2, 11–13]. The main drawbacks of alumina are the formation of chromia–alumina solid solutions varying in their crystal structure and its high surface acidity, which gives rise to side reactions (cracking and the formation of hardly burnable coke on the catalyst surface) [13, 14].

Along with the γ-Al_2O_3-supported catalysts, there are chromium oxide catalysts supported on SiO_2, ZrO_2, and TiO_2 [15–17] and on mesoporous ordered materials [18–20]. Silica gel has a more developed porous structure than alumina and a low inherent catalytic activity. However, chromium in its higher oxidation states is poorly stabilized on the silica surface, which leads to formation of α-Cr_2O_3 particles [20], which show a low dehydrogenating activity. The highest activity in dehydrogenation is exhibited by ZrO_2-supported chromium catalysts because chromium oxides on the zirconia surface are stabilized in the highly dispersed state [21]. However, use of Cr/ZrO_2 catalysts is limited by the expensiveness of zirconium compounds, difficulty to obtain a support with a large specific surface area, and low stability of porous structure to high-temperature heat treatment [22].

Thus, the properties of the support surface define the chemical state of the supported chromium and, accordingly, its catalytic activity. Large part of the chromium on the alumina or zirconia surface is in the highly dispersed hexavalent state. The ratio of chromium in the form of CrO_3 to chromium in the form of chromates depends also on the amount of alkali metal dopant potassium or sodium [23, 24]. Correlations

were established between the activity of chromium-containing catalysts and the proportion of reversibly oxidizable/reducible chromium, which depends on the nature of the support and on the alkali metal content [25]. At the same time, it is essential for a commercial catalyst be produced as granules with a specified porous structure (that would ensure efficient reactant transport and product removal), strength and a high thermal stability. This imposes serious limitations on the use of some highly active catalytic systems, including Cr/ZrO_2 catalysts. Therefore, it is important to develop mixed supports that would have a developed porous structure, high chemical and thermal stability low surface acidity and ability to form active phase of chromium oxides.

In the present work an approach to obtain ZrO_2–SiO_2 mixed supports combining the developed porous structure of silica gel and the functional properties of the zirconia surface that are necessary for stabilizing supported chromium in its active state was suggested. Also, the state of chromium on the surface of silica doped with zirconia and the catalytic properties of the synthesized model chromium-containing catalysts in isobutane dehydrogenation were studied.

EXPERIMENTAL

Synthesis of Supports and Catalyst

The primary support for catalyst preparation was commercial mesoporous silica gel (KSKG brand, Russia). To increase the pore size, the silica gel was hydrothermally treated with aqueous ammonia solution [27] and dried at 600°C for 4 h to remove ammonia and water.

Silica-based supports doped with zirconia were obtained by the incipient-wetness impregnation of silica gel with an aqueous solution of $ZrO(NO_3)_2 \cdot H_2O$ stabilized by citric acid (Zr : citric acid = 1 : 2). The impregnated samples were dried at 80°C for 12 h and were then calcined at 600°C for 4 h. In this way, we synthesized a series of ZrO_2–SiO_2 supports containing 0.5, 1.0, and 2.0 monolayers (ML) of ZrO_2 (under the assumption that the monolayer capacity is 5 atoms Zr/nm^2 support [28]) or, correspondingly, 5.2, 10.4, and 20.8 wt % ZrO_2. These samples will be designated as $0.5ZrO_2$–SiO_2, $1.0ZrO_2$–SiO_2, and $2.0ZrO_2$–SiO_2, respectively.

The ZrO_2 support was synthesized by the thermal decomposition of $ZrO(NO_3)_2 \cdot H_2O$ at 600°C for 4 h.

The supports thus obtained were subjected to incipient-wetness impregnation with an aqueous solution of CrO_3 (reagent grade) and KNO_3 (K : Cr = 1 : 5 mol/mol) to synthesize model chromium-containing catalysts with one chromium monolayer (5 atoms Cr/nm^2 support) [21] or, correspondingly ~1.5 wt % Cr for CrO_x/ZrO_2 and 4.4–5.2 wt % Cr for the silica-based samples. The resulting catalysts were dried at 80°C for 12 h and were then calcined in air at 600°C for 4 h.

Characterization of Supports and Catalysts

The porous structure of the materials was characterized by nitrogen adsorption at –196°C on a TriStar 3020 automated gas adsorption analyzer (Micromeritics, United States). The specific surface area was determined by the multipoint BET method via linearization of the adsorption isotherm in the P/P_0 range from 0.05 to 0.30. The pore size distribution function was constructed by the BJH-desorption method with an analysis of the desorption branch of the nitrogen adsorption–desorption isotherm. Prior to taking measurements, the sample (100–120 mg) was degassed in a vacuum at 200°C for 2 h.

The chemical state of chromium and the phase composition of the catalysts were studied by diffuse reflectance spectroscopy (DRS) or UV–vis spectroscopy and X-ray diffraction (XRD). Diffuse reflectance spectra were recorded on an Evolution 600 spectrometer (Thermo Scientific, United States). XRD patterns were obtained on a Miniflex 600 diffractometer (Rigaku, Japan) using monochromatic CuK_α radiation (λ = 1.5418 Å) under the following conditions: scanning speed of 0.2 deg/min, step size of 0.2 deg, $2\theta = 10°$–$90°$. The phase composition of catalysts was determined using the PCPDFWIN database and the POWDER CELL 2.4 full-profile analysis program.

Temperature-programmed reduction with hydrogen (H_2-TPR) was carried out on a ChemiSorb 2750 chemisorption analyzer (Micromeritics) with a thermal-conductivity detector (TCD signal) at a heating rate of 10 deg/min in a flow of argon–hydrogen mixture (10 vol % H_2, flow rate of 20 mL/min).

Catalytic Tests

The activity of the synthesized catalysts was tested in isobutane dehydrogenation in a tubular quartz flow reactor with a fixed catalyst bed at 540°C. The feed, which consisted of 15% i-C_4H_{10} and N_2 balance gas, was passed through the catalyst bed at a rate of 1.8 L/h (540 h^{-1}). The weight of the catalyst sample was 200–300 mg. A test was performed for 2 h, with the product gas sampled at 15-min intervals. The gaseous products of the reaction were analyzed on Chromatec-Crystall 5000.2 gas chromatograph (Chromatec, Russia) with a thermal-conductivity detector, two flame-ionization detectors, and a Varian Capillary Column CP-Al_2O_3/Na_2SO_4 capillary column (50 m) at 130°C. The components of the gas mixture were quantified using the Chromatec-Analytic 2.6 software by an absolute calibration method involving a calibration gas mixture. The mixture was standardized according to the Primary Standard GET 154-2001 in compliance with the RF State Standard GOST 8.578-2002 concerning gas standardization.

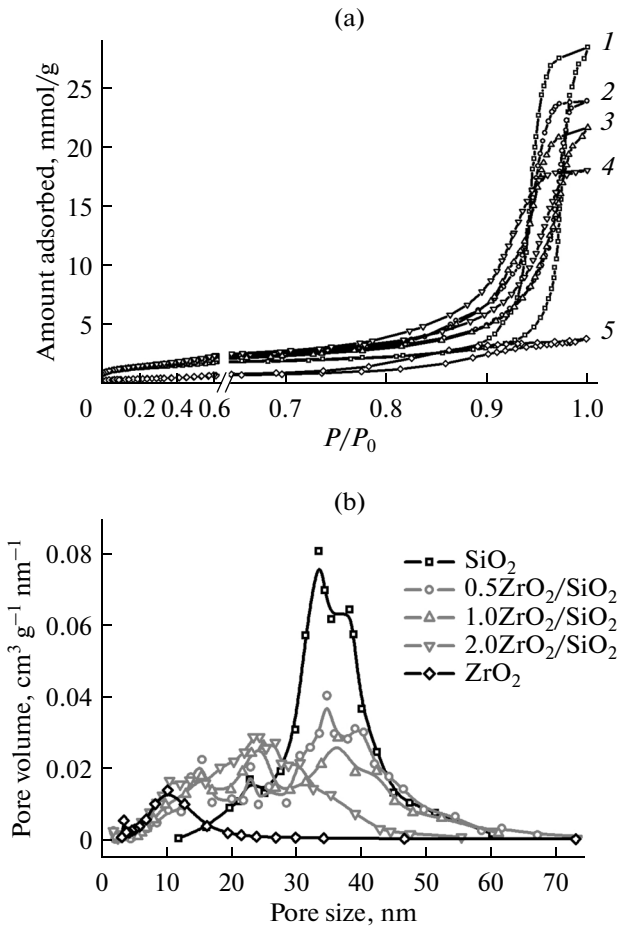

Fig. 1. (a) Nitrogen adsorption–desorption isotherms and (b) pore size distribution for the (*1*) SiO_2, (*2*) $0.5ZrO_2$–SiO_2, (*3*) $1.0ZrO_2$–SiO_2 (*4*) $2.0ZrO_2$–SiO_2, and (*5*) ZrO_2 supports.

RESULTS AND DISCUSSION

Catalyst Characterization

The porous structure of the synthesized supports was investigated by low-temperature nitrogen adsorption. Figure 1 shows nitrogen adsorption–desorption isotherms and pore size distribution for the SiO_2, ZrO_2, and ZrO_2–SiO_2 supports. The isotherm for the initial silica gel has a hysteresis loop in the relative pressure range from 0.9 to 1.0, indicating that SiO_2 has a mesoporous structure (Fig. 1a). From the pore size distribution one can see that the porous structure of the silica gel consists of large 20 to 50 nm mesopores (Fig. 1b). The nitrogen adsorption–desorption isotherm for zirconia has a hysteresis loop in the relative pressure range from 0.75 to 0.97 indicating that the zirconia sample has a mesoporous structure. However, unlike the porous structure of SiO_2, the porous structure of ZrO_2 is dominated by 3–20 nm mesopores. In the nitrogen adsorption–desorption isotherms for the series of zirconia-doped silica gels, the hysteresis intensity in the relative pressure range from 0.9 to 1.0 decreases, and the hysteresis loop shifts to the 0.75–0.9 region indicating a decrease in the proportion of large (20–50 nm) mesopores and an increase in the proportion of smaller mesopores. It follows from the pore size distribution data that for the ZrO_2–SiO_2 samples the dominant pore diameter decreases with an increasing ZrO_2 content. For the sample containing 2 ML of ZrO_2, the volume of 30–50 nm pores is insignificant.

Table 1. Properties of supports

Support	S_{BET}, m^2/g	V_{pore}, cm^3/g	D_{pore}, nm*
SiO_2	102	0.99	33.7
$0.5ZrO_2/SiO_2$	115	0.83	27.2
$1.0ZrO_2/SiO_2$	110	0.73	25.0
$2.0ZrO_2/SiO_2$	120	0.63	19.1
ZrO_2	34	0.13	10.7

* Determined by the BJH-desorption method.

The specific surface area, and pore volume and size data for the synthesized supports are listed in Table 1. The initial silica gel has a specific surface area of 102 m^2/g, a pore volume of 0.96 cm^3/g, and an average pore diameter of 33.7 nm. The specific surface area of the ZrO_2 sample is 34 m^2/g, its total pore volume is 0.13 cm^3/g, and its average pore diameter is 10.7 nm. Thus, the SiO_2 and ZrO_2 supports differ significantly in their porous structure. Doping the silica gel with zirconia slightly increases its specific surface area and decreases its pore volume because of the filling of pores by zirconia. The synthesized ZrO_2–SiO_2 supports have a large specific surface area and a developed system of wide transport mesopores. This makes them promising for chromium-containing catalysts.

The chemical state of chromium on the surface of the synthesized supports was studied by XRD and DRS. Figure 2a shows the XRD patterns of the synthesized chromium-containing catalysts. For all of the silica-based samples, there is an extensive halo in the $2\theta = 10°$–$35°$ region, which is due to the amorphous structure of the silica gel. For the catalysts supported on zirconia-doped silica gel, the diffraction patterns show reflections from cubic and monoclinic ZrO_2 phases, the former being dominant (strongest reflections at $2\theta = 30.2°$, 50.4°, and 60.0°). The intensity of the reflections increases with an increasing zirconia content of the catalyst. As this takes place, the crystallite size of cubic ZrO_2 (determined using the Scherrer equation) does not increase and is 4.1–4.4 nm (Table 2). Thus, doping silica gel with zirconia yields ZrO_2 crystallites that fill the pore space of the silica gel. This increases the specific surface area but reduces the pore volume and narrows the pores (Fig.1, Table 1).

The XRD patterns of all of the silica-based catalysts show reflections from the α-Cr_2O_3 phase, and the intensity of these reflections decreases as the ZrO_2

content is increased from 0 to 2 ML. However, calculation of the coherent scattering region size demonstrated that the Cr_2O_3 crystallite size in these samples is practically invariable and is 26–29 nm (Table 2). The weakening of the reflections can be either due to the decrease in the proportion of the Cr_2O_3 phase or number of large particles, which make the main contribution to the reflection intensity.

The XRD patterns of the CrO_x/ZrO_2 catalyst show only reflections from the zirconia phases, mainly from the cubic one. The crystallite size of cubic ZrO_2 is 18 nm (Table 2). Because many of the reflections from the zirconia phases are overlapped with reflections from α-Cr_2O_3, we present an enlarged diffraction pattern in the $2\theta = 33°–38°$ region (inset in Fig. 2a), from which it is clear that, the background of reflections from cubic and monoclinic ZrO_2, does not contain two strongest reflections from α-Cr_2O_3 ($2\theta = 33.61°$ and 36.20°). Thus, no reflections from chromium-containing phases are observed for this sample indicating that the entire chromium is in the highly dispersed, X-ray-amorphous state.

The DRS spectra of the synthesized catalysts (Fig. 2b) show absorption bands with maxima at 360–380, 460, and 600 nm. Absorption in the wavelength range from 320 to 420 nm is assignable to hexavalent chromium that is mainly in the form of chromates (tetrahedral coordination). The doublet in the visible region is due to Cr(III) in the form of Cr_2O_3 (octahedral coordination) [19, 21, 28]. This band assignment is confirmed by the DRS spectra of the Cr_2O_3, CrO_3, K_2CrO_4, and $K_2Cr_2O_7$ compounds (their spectra are not presented here).

The DRS spectrum of the CrO_x/ZrO_2 catalyst shows an absorption band at 380 nm and no absorption in the long-wavelength spectral region. Therefore, the major part of chromium in this catalyst is in the hexavalent state, and this accounts for the absence of reflections from α-Cr_2O_3 in the XRD pattern. The absence of reflections from Cr(VI)-containing phases indicates that these phase are in a highly dispersed state. (The formation of a near-monolayer coating is not ruled out.) At the same time, the DRS spectra of the catalysts supported on the initial and zirconia-modified silica gel show absorption due to both Cr_2O_3 and hexavalent chromium. Note that with an increasing proportion of zirconia introduced, the absorption bands characterizing Cr(III), occurring at 460 and 600 nm, weaken, and the absorption band at 280–360 nm, which indicates the presence of Cr(VI), strengthens. This fact correlates with the weakening of reflections from α-Cr_2O_3 in the XRD patterns of these catalysts.

The H_2-TPR profiles for the synthesized Cr-containing catalysts are presented in Fig. 3. For all of the catalysts, the TPD profiles indicate a hydrogen uptake at 350–550°C, which is evidence of Cr(VI) reduction to Cr_2O_3 [6, 19]. The hydrogen uptake at 400–550°C for the CrO_x/SiO_2 is possibly due to the reduction of potassium chromates [23, 28, 29]. For the samples

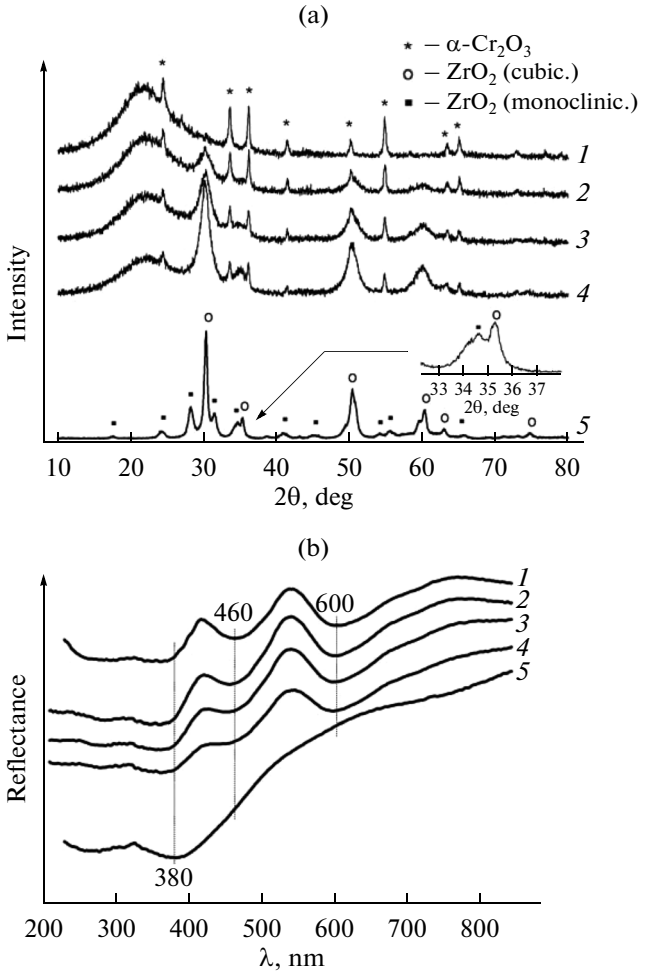

Fig. 2. (a) X-ray diffraction patterns and (b) DRS spectra of the synthesized chromium-containing catalysts: (*1*) CrO_x/SiO_2, (*2*) $CrO_x/0.5ZrO_2–SiO_2$, (*3*) $CrO_x/1.0ZrO_2–SiO_2$ (*4*) $CrO_x/2.0ZrO_2–SiO_2$, and (*5*) CrO_x/ZrO_2. Inset: enlarged diffraction pattern in the $2\theta = 32°–38°$ region.

based on modified silica gel, the intensity of the hydrogen uptake peak increases with an increasing ZrO_2 content and the peak itself shifts to lower temperatures.

Chromium reduction in the CrO_x/ZrO_2 catalyst is observed at 250–450°C indicating that chromium is reduced from the Cr(VI) state [23, 28, 29]. However, it was demonstrated by EPR spectroscopy [21] that when the ZrO_2 surface contains a small amount of chromium (<1 ML), up to 50% of the chromium can be in the form of mononuclear Cr(V) species. A specific feature of this state of chromium is that it is detectable only by EPR, not by XRD or DRS. However, this state should not be ignored because, according to the literature [21], it is the reduction of Cr(V) that yields isolated Cr^{3+} sites that show the highest activity in the dehydrogenation of paraffin hydrocarbons, including isobutane. Thus, the observed hydrogen uptake peaks can be assigned to the reduction of both Cr(VI) and Cr(V). The shift of the hydrogen

Table 2. Properties of the synthesized catalysts

Catalyst	Cr, wt %	$D(ZrO_2)$, nm	$D(Cr_2O_3)$, nm	H_2 uptake, mol H_2/mol Cr*	Activity**		
					(mmol i-C_4H_{10}) g_{Cat}^{-1} s^{-1}	(mol i-C_4H_{10}) (mol Cr)$^{-1}$ s^{-1}	S, %
CrO_x/SiO_2	4.4	–	29	0.32	0.1	0.09	72
$CrO_x/0.5ZrO_2–SiO_2$	5.0	4.1	26	0.45	1.3	1.63	96
$CrO_x/1.0ZrO_2–SiO_2$	4.7	4.1	29	0.55	2.0	2,54	97
$CrO_x/2.0ZrO_2–SiO_2$	5.2	4.4	27	0.63	2.6	3.24	98
CrO_x/ZrO_2	1.5	18	–	0.92	1.6	5.85	99

S is the isobutene formation selectivity.

* TPR data.

** In the 15th minute of the catalytic test.

uptake peak for CrO_x/ZrO_2 to lower temperatures may be due to the fairly large proportion of Cr(V) in this sample.

The decrease in the reduction temperature in the series of $CrO_x/ZrO_2–SiO_2$ catalysts can be explained by the participation of the ZrO_2 phase in the stabilization of pentavalent and hexavalent chromium in the highly dispersed state. Converting the TPR peak areas to the amount of hydrogen consumed demonstrates (Table 2) that with an increasing ZrO_2 content of the catalyst the hydrogen uptake increases from 0.32 to 0.92 mol H_2/mol Cr for the CrO_x/SiO_2 and CrO_x/ZrO_2 samples, respectively. This indicates that the proportion of pentavalent and hexavalent chromium increases from 21–32% (depending on the Cr(V) : Cr(VI) ratio) for the CrO_x/SiO_2 catalyst to 61–92% for the CrO_x/ZrO_2 catalyst. The effects observed by the TPR method are in good agreement with our DRS and XRD data (Fig. 2).

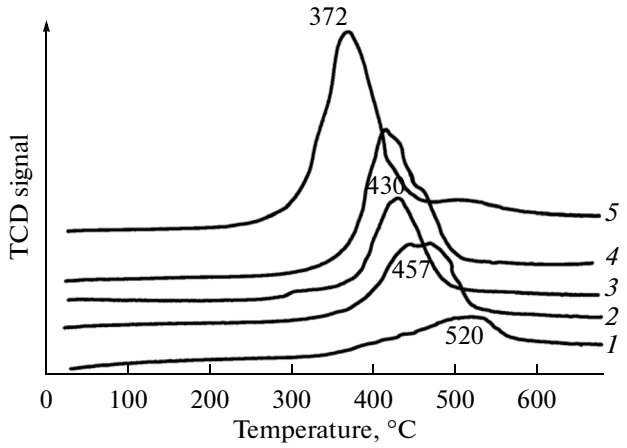

Fig. 3. H_2-TPR profiles for the (*1*) CrO_x/SiO_2, (*2*) $CrO_x/0.5ZrO_2–SiO_2$, (*3*) $CrO_x/1.0ZrO_2–SiO_2$, (*4*) $CrO_x/2.0ZrO_2–SiO_2$, and (*5*) CrO_x/ZrO_2 catalysts.

Catalytic Activity

The catalytic properties of the synthesized Cr-containing catalysts were studied in isobutane dehydrogenation in a fixed catalyst bed. Figure 4 plots the time dependence of catalytic activity over the 15–120 min range. The highest activity (in terms of isobutane conversion rate per mole of Cr in the catalyst) is displayed by the CrO_x/ZrO_2 sample. The CrO_x/SiO_2 catalyst is much inferior in activity to CrO_x/ZrO_2. The zirconia-modified catalysts $CrO_x/ZrO_2–SiO_2$ are considerably more active and more selective than the undoped catalyst CrO_x/SiO_2 (Table 2). In terms of isobutane conversion rate per weight of catalyst (Table 2), the $CrO_x/ZrO_2–SiO_2$ samples containing 1 or 2 ML of zirconia are more active than the CrO_x/ZrO_2 catalyst.

Correlating the results of investigation of the chemical state of supported chromium with the catalytic properties of the synthesized Cr-containing catalysts revealed the following regularities. Relatively large particles of the α-Cr_2O_3 phase form on the silica gel surface. This phase exhibits low activity in isobutane dehydrogenation, including because of its low degree of dispersion, i.e., because of the low concentration of surface Cr atoms involved in the reaction. The entire chromium in the CrO_x/ZrO_2 catalyst is in the highly dispersed, X-ray-amorphous state dominated by pentavalent and hexavalent chromium (according to DRS and TPR data). According to the TPR data, chromium in this catalyst is rather readily reducible presumably from the Cr(V) and CrO_3 states, while hexavalent chromium in the CrO_x/SiO_2 catalyst is stabilized by potassium presenting in the catalyst to yield potassium chromates. In the CrO_x/ZrO_2 catalyst, the reduction of pentavalent and hexavalent chromium yields highly dispersed, X-ray amorphous chromium(III) oxide clusters, which make the catalyst very active in isobutane dehydrogenation.

The proportion of large Cr_2O_3 particles in the $CrO_x/ZrO_2–SiO_2$ catalysts decreases with an increasing proportion of Cr(VI) and, possibly, with an increasing proportion of Cr(V) species stabilized by the zirconia surface. An increase in the proportion of

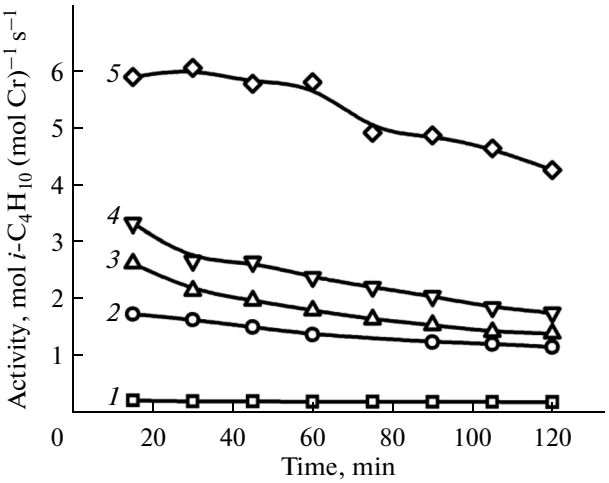

Fig. 4. Activity of catalysts in isobutane dehydrogenation as a function of on-stream time: (*1*) CrO_x/SiO_2, (*2*) $CrO_x/0.5ZrO_2–SiO_2$, (*3*) $CrO_x/1.0ZrO_2–SiO_2$, (*4*) $CrO_x/2.0ZrO_2–SiO_2$, and (*5*) CrO_x/ZrO_2.

pentavalent and hexavalent chromium leads to a marked increase in the activity and selectivity of the catalyst in isobutane dehydrogenation into isobutene.

CONCLUSIONS

Modification the silica gel surface with zirconia affords a support with a larger specific surface area (Table 1) and with surface properties ensuring stabilization of supported chromium in the highly dispersed very active state. The approach suggested here provides means to obtain mixed oxide supports combining the properties of silica gel (developed porous structure, thermal stability, relative inertness) with the properties of zirconia that stabilize chromium in the highly dispersed state, ensuring a high isobutane dehydrogenation activity of the catalyst. The catalysts prepared using this approach are free of the drawbacks inherent in zirconia-supported catalysts, such as a small specific surface area and agglomeration at high temperatures, and they are less expensive owing to the lower zirconia content. Based on this approach, we are going to synthesize catalysts with a higher active component content and compare these catalysts with commercial chromia–alumina catalysts under conditions close to industrial catalyst operation.

ACKNOWLEDGMENTS

We thank Dr. S.A. Kuznetsova for XRD studies. This work was supported through the federal target program "Research and Development in the Priority Areas of the Science and Technology Complex of Russia for 2014–2020" (contract no. 14.578.21.0028).

REFERENCES

1. RF Patent 2373175, 2008.
2. RF Patent 2322290, 2008.
3. Pakhomov, N.A., Kashkin, V.N., Nemykina, E.I., Molchanov, V.V., Nadtochiy, V.I., and Noskov, A.S., *Chem. Eng. J.*, 2009, vol. 154, p. 185.
4. Elbashir, N.O., Al-Zahrani, S.M., Abasaeed, A.E., and Abdulwahed, M., *Chem. Eng. Process.*, 2003, vol. 42, p. 817.
5. Neri, G., Pistone, A., De Rossi, S., Rombi, E., Milone, C., and Galvagno, S., *Appl. Catal., A*, 2004, vol. 260, p. 75.
6. Hardcastle, F.D. and Wachs, I.E., *J. Mol. Catal.*, 1988, vol. 46, p. 173.
7. Indovina, V., *Catal. Today*, 1998, vol. 41, p. 95.
8. Harlin, M.E., Niemi, V.M., and Krause, A.O.I., *J. Catal.*, 2000, vol. 195, p. 67.
9. Gueguen, E., Delsarte, S., Peltier, V., Conanec, R., Marchand, R., Laurent, Y., and Grange, P., *J. Eur.. Ceram. Soc.*, 1997, vol. 17, p. 2007.
10. Ohta, M., Ikeda, Y., and Igarashi, A., *Appl. Catal., A*, 2004, vol. 258, p. 153.
11. RF Patent 2148430, 2000.
12. RF Patent 2200143, 2003.
13. Pakhomov, N.A., Parakhin, O.A., Nemykina, E.I., Danilevich, V.V., Chernov, M.P., and Pecherichenko, V.A., *Catal. Ind.*, 2012, vol. 4, p. 298.
14. Fridman, V.Z., *Appl. Catal., A*, 2010, vol. 382, p. 139.
15. Vuurman, M.A., Wachs, I.E., Stufkens, D.J., and Oskam, A., *J. Mol. Catal.*, 1993, vol. 80, p. 209.
16. Sloczynski, J., Grzybowska, B., Kozlowska, A., Samson, K., Grabowski, R., Kotarba, A., and Hermanowska, M., *Catal. Today*, 2011, vol. 169, p. 29.
17. Ma, F., Chen, S., Wang, Y., Chen, F., and Lu, W., *Appl. Catal., A*, 2012, vol. 427, p. 145.
18. Xu, L., Wang, Z., Song, H., and Chou, L., *Catal. Commun.*, 2013, vol. 35, p. 76.
19. Shee, D. and Sayari, A., *Appl. Catal., A*, 2010, vol. 389, p. 155.
20. Takehira, K., Ohishi, Y., Shishido, T., Kawabata, T., Takaki, K., Zhang, Q., and Wang, Y., *J. Catal.*, 2004, vol. 224, p. 404.
21. De Rossi, S., Casaletto, M.P., Ferraris, G., Cimino, A., and Minelli, G., *Appl. Catal., A*, 1998, vol. 167, p. 257.
22. Rezaei, M., Alavi, S.M., Sahebdelfar, S., and Zi-Feng Yan, *Powder Technol.*, 2006, vol. 168, p. 59.
23. Rombi, E., Cutrufello, M.G., Solinas, V., De Rossi, S., Ferraris, G., and Pistone, A., *Appl. Catal., A*, 2003, vol. 251, p. 255.
24. Nesterov, O.N., Egorova, S.R., Bekmukhamedov, G.E., Kataev, A.N., Lamberov, A.A., and Gil'manov, Kh.Kh., *Vestn. KGTU*, 2011, vol. 9, p. 33.
25. Puurunen, R.L. and Weckhuysen, B.M., *J. Catal.*, 2002, vol. 210, p. 418.
26. Dutov, V.V., Mamontov, G.V., and Vodyankina, O.V., *Izv. Vyssh. Uchebn. Zaved., Fiz.*, 2011, no. 12/2, p. 21.
27. Korhonen, S.T., Airaksinen, S.M.K., Banares, M.A., and Krause, A.O.I., *Appl. Catal., A*, 2007, vol. 333, p. 30.
28. Cutrufello, M.G., De Rossi, S., Ferino, I., Monaci, R., Rombi, E., and Solinas, V., *Thermochim. Acta*, 2005, vol. 434, p. 62.
29. Gaspar, A.B. and Dieguez, L.C., *Appl. Catal., A*, 2002, vol. 227, p. 241.

Translated by D. Zvukov